ACS OMEGA

Open Access

http://pubs.acs.org/journal/acsodf

Article

New Insight into Elastic Mechanical Properties and Anisotropies of Crystal Defect α-Quartz from DFT Calculation

Lin Zhang, Fen Jiao,* Wenqing Qin, and Qian Wei

Cite This: *ACS Omega* 2023, 8, 43644−43650

Read Online

ACCESS | Metrics & More | Article Recommendations | Supporting Information

ABSTRACT: To reveal the cleavage mechanism of α-quartz in the grinding process of nonferrous metal ores, mechanical and charge properties of α-quartz crystals are investigated using the density functional theory. Based on the elastic constant matrix, the bulk and shear moduli were calculated before and after the α-quartz with oxygen atom defects. The results show that the ratios of bulk and shear moduli (B/G) were 0.87 and 0.95, respectively, which indicated that at the same stress level, it was easier to fracture without O-vacancy defects than with O-vacancy defects. The mapping surfaces indicated that the O-vacancy defect increased the bulk-, shear-, and Young's moduli, and Poisson ratio while decreasing the hardness. The anisotropy index (A_L and A^U) was calculated which illustrated that the O-vacancy can result in an increased anisotropy; meanwhile, the bulk anisotropy index (A_B) increased strongly about two times. The anisotropy analysis shows the dominance crystal cleavage of the (011) plane in the shear stress and the dominance crystal cleavage of the (111) plane in the normal stress. The electron localization function α-quartz show that the O-vacancy defect can decrease the Si−Si length from 3.703 to 2.442 Å, which indicated that the O-vacancy formed the new covalent bonds between silicon atoms. Our work provided a systematic approach containing the mechanical, anisotropic, and electronic properties of mineral crystals to explain the cleavage behavior of crystals.

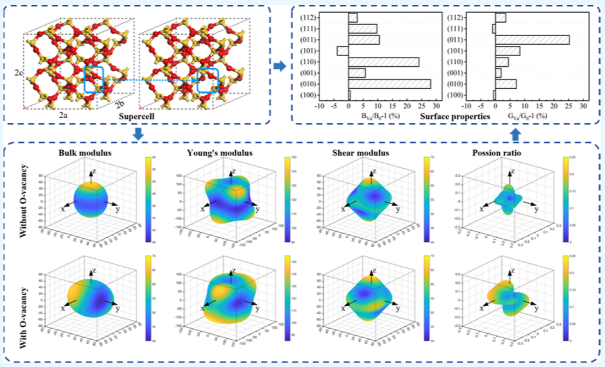

1. INTRODUCTION

Quartz, an abundant mineral on Earth, often is a gangue in paragenesis with strategic mineral resources such as lepidolite, cassiterite, sphalerite, and galena.[1] The broad definition of quartz also includes α-quartz, besides including β-quartz and coesite. α quartz is the dominant mineral in a variety of rock types, including sedimentary, metamorphic, and igneous rocks.[2] The presence of quartz leads to the excessive crushing of the target minerals, resulting in the loss of approximately 10 to 20% of valuable metallic minerals per year[3] and also leads to higher energy consumption for grinding. Separating valuable metallic mineral resources from quartz is a significant challenge due to its sturdy and tough structure that resists crushing and grinding. Vieira et al.[4] studied the floatability of quartz particles with different particle sizes in the flotation separation process of itabirite. Zhou et al.[5] also studied the effect of particle size on the flotation separation process of quartz. The results showed that when the particle size was below 0.030 mm, the flotation separation effect was poor. Feng et al.[6] studied the effect of calcium ions on the flotation process of quartz and cassiterite. The results showed that when the pH value was around 8.2, the floatability of quartz was less than that of cassiterite. Xie et al.[7] studied the effects of Ca(II), Mg(II), Fe(II, III), and plasma on the flotation separation process of quartz and spodumene, and the results showed that $Fe(OH)_3$ was preferentially adsorbed on quartz. Nonetheless, understanding the physical and mechanical traits of quartz is critical to studying mineral flotation, which requires the dissociation of monomers of the target mineral.

At present, the research on macroscope mechanical behavior such as compressive strength, shear strength, and so on, mainly studied limestone, sandstone, and other ores.[8−10] However, in the procession of separation and purification, the minerals need further crushing and grinding for monomeric dissociation (below the micron scale). Choyal et al.[11,12] investigated the vacancy on the elastic coefficient and Young's modulus and shear modulus of boron nitride nanotubes (BNNTs) and revealed the critical role played by vacancy defected BNNTs in determining the elastic properties and electronic properties of BNNTs. Kothari et al.[13] also indicated that vacancy defects are the main factor affecting the thermal conductivity of carbon nanotubes CNTs. With the particle size of quartz minerals decreasing below microns, the properties of macroscopic cleavage cannot accurately characterize the mechanical proper-

Received: July 18, 2023
Revised: October 11, 2023
Accepted: October 13, 2023
Published: November 8, 2023

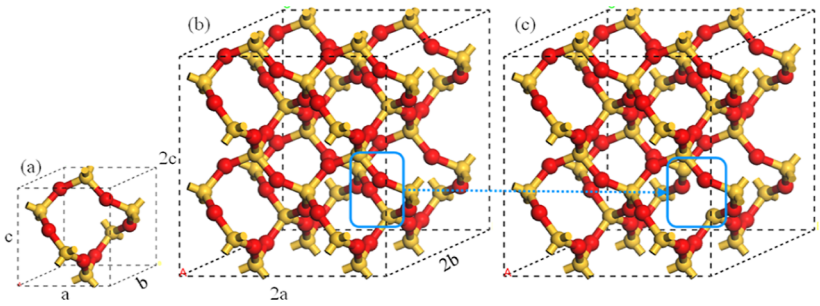

Figure 1. α-Quartz crystal structure unit cell (a), supercell without (b), and supercell with (c) an O-vacancy defect. The in-cell style box indicates the position of the defect, the red spheres represent oxygen atoms, and yellow spheres represent silicon atoms.

Table 1. Calculated Elastic Constants of α-Quartz

		C_{11}/GPa	C_{12}/GPa	C_{13}/GPa	C_{14}/GPa	C_{33}/GPa	C_{44}/GPa	C_{66}/GPa
unit cell	this paper	104.08	9.77	21.43	−9.39	107.42	65.40	47.15
	ref 18	87.26	6.57	11.95	−17.18	105.8	57.15	40.35
supercell (2 × 2 × 2)	this paper	101.87	9.21	19.66	−10.73	109.68	68.60	46.32
	O-vacancy	106.85	9.76	21.82	−8.25	110.60	74.39	49.38

Table 2. Calculated Mechanical Properties of α-Quartz[a]

	unit cell			without O-vacancy			with O-vacancy		
	voigt	reuss	hill	voigt	reuss	hill	voigt	reuss	hill
bulk modulus	46.76	46.56	46.66	45.61	45.31	45.46	52.58	51.43	52.00
shear modulus	53.12	50.03	51.58	54.36	50.49	52.42	56.94	52.54	54.74
Young's modulus	115.60	110.51	113.07	116.72	110.45	113.61	125.52	117.59	121.57
Poisson ratio	0.088	0.104	0.073	0.073	0.094	0.083	0.102	0.119	0.110
hardness*		16.81			17.85			16.59	
hardness**		19.58			20.95			19.08	
β		0.022			0.027			0.019	
B/G		0.90			0.87			0.95	

[a]The unit of bulk-, shear-, Young's modulus in GPa, β in GPa^{-1}. The * was calculated by Tian,[26] and the ** was calculated by Chen.[27]

ties of the quartz crystal; instead, the crystal structure of minerals will have an increasing influence on the mechanical properties and lattice defect of mineral crystals.[14] The fundamental defects in both crystalline and alpha SiO_2 have been studied intensely for decades. The oxygen vacancy is important and has also been formed to the fundamental positive charge trap in bulk.[15] The crystal point defects lead to the deflection of electrons, which can also influence the electron properties of a pulp in the grinding or floatation process. The crystal mechanical property of metal materials has been conducting numerous studies; meanwhile, the mechanical property of nonmetallic minerals on a crystal scale has become a hot-spot field gradually. Yuan et al.[16] and Zhang et al.[17] studied the mechanical properties and fracture surface of Siderite and hematite, which revealed that the defects did not affect the symmetry of the distribution of mechanical properties. Heyliger et al.[18] measured the elastic constant of a natural quartz sphere via resonance-ultrasound spectroscopy. The research focuses on the properties of unit cell, but the influence of quartz crystal defects on mechanical properties and crystal anisotropy is studied less.

In this work, the mechanical properties and anisotropies of α-quartz with and without O-vacancy defects were studied by DFT. The supercell method was used to control the defect concentration at a reasonable level and to eliminate the influence of interaction among defects. The mechanical properties of the crystal such as the bulk, shear, and Young's moduli were calculated via the elastic constant matrix. The spatial distributions of Young's modulus, shear modulus, and Poisson ratio on the crystal were mapped to illustrate the elastic anisotropy and the grindability. The distribution of electron density function and electron localization function (ELF) reveal the effect of crystal electron properties with and without the O-vacancy defect. This research into crystalline mechanical properties will provide new insights into the relationship between mechanical properties and fracture surfaces.

2. RESULTS AND DISCUSSION

2.1. Defect Energy. For ensuring the accuracy of the simulation, the O-vacancy defect crystal was built in a supercell consisting of a defect surrounded by dozens of atoms of the host minerals. Although the use of an array of defects may lead to artificial interactions between the defects, these artifacts become negligibly small when the supercell size is sufficiently increased. In this work, the defect-bearing α-quartz was constructed with large lattice sizes and low concentrations of defects.

As shown in Figure 1b,c, the with and without the O-vacancy defect 2 × 2 × 2 supercell of α-quartz crystals both consisted of 72 atoms, comprising 24 silicon atoms and 48 oxygen atoms, which belong to the space group rhombohedral.

https://doi.org/10.1021/acsomega.3c05173
ACS Omega 2023, 8, 43644−43650

The supercell was created by extending the *a*, *b*, and *c* crystal lattices of the unit cell. The unit cell of α-quartz has lattice constants of $a = b = 4.93975$ Å and $c = 5.43625$ Å, while after extending the lattice, the dimensions of the supercells reached $a = b = 9.87893$ Å, $c = 10.8915$ Å, which reduced the interaction between the defects. The O-vacancy defects in α-quartz were calculated to have formation energies of 5.69 eV, which is consistent with the result of others.[28−30]

The optimized α-quartz with an O-vacancy defect is shown in Figure 1c. The in-cell style shows the distribution of the O-vacancy in the crystal. The defect concentrations of α-quartz were 1.39%. After the geometry optimization, the lattice parameters were smaller than those in the perfect crystal. This distortion of the cell geometry led to a change of crystal symmetry such that the space group of α-quartz with defects changed to *P*1.

2.2. Elastic Property. The elastic constants of the unit cell and supercell of α-quartz were calculated. As shown in Table 1, the elastic constants of the α-quartz were somewhat different from those of the unit cells. Almost all the elastic constants of the supercells were smaller than the unit cell, due to the different settings of *k*-points and the crystal boundary effects. Nonetheless, the differences between the supercell and unit cell values were within the maximum error requirement and the values showed the same trend, which suggests the reliability of these calculation results.

The bulk modulus and shear modulus of the α-quartz can be calculated with elastic constants. The mechanical properties are shown in Table 2. The bulk modulus (B) of the unit cell and without an O-vacancy, a supercell, is a few changes that are 46.66 and 45.46 GPa, respectively. Regardless of the existence or absence of the defects of the O-vacancy, the shear modulus values are larger than the bulk modulus, which means that the α-quartz with the O-vacancy has stronger mechanical stability than that without O-vacancy.

B/G and Poisson ratio can be used to weigh the ductile or brittle materials. The value of B/G which distinguishes ductile and brittle minerals is about 1.75.[17,31] The value (B/G) of the unit cell, supercell without an O-vacancy, and supercell with an O-vacancy are 0.90, 0.87, and 0.95, respectively. This indicates that the O-vacancy defect increases the ductile slightly, while they still are brittle minerals. Meanwhile, for the brittle covalent materials, it is about 0.1, and for the ductile metallic materials, it is about 0.33. The Poisson ratio of the α-quartz crystal (supercell without O-vacancy and supercell with O-vacancy) is 0.083 and 0.110, respectively. This illustrates that the O-vacancy defect would increase the brittleness of the α-quartz crystal. The hardness of α-quartz using eqs 11 and 12 is shown in Table 2. The results of two way calculation show the same tendency that the hardness of the O-vacancy defect decreases slightly.

2.3. Elastic Anisotropy. Elastic anisotropy determines many basic properties of minerals and is important for predicting the fracture toughness of minerals. The universal anisotropy index A^U and percent anisotropy indices of compression and shear (A_B and A_G) are used to evaluate the α-quartz. As shown in Table 3, if the values of A^U, A_B, and A_G equal zero, the crystal is isotropic. The greater their deviation from 0, the higher the degree of anisotropy.

The mapping surfaces of the mechanical properties are shown in Figure 2. The surfaces demonstrate how the Young's modulus, shear modulus, and Poisson ratio vary with crystallographic direction. The points of the surface represent the magnitude of Young's modulus, shear modulus, and Poisson ratio in the direction of a vector from the origin to a given point on the surface. Figures 2a,e and 3d,h show clearly that the mapping surfaces of α-quartz mechanical properties which are the unit cell and supercell without an O-vacancy defect are similar. We can discuss the influence of the supercell without or with O-vacancy defect. The bulk modulus of the O-vacancy defect is enlarged along the *z*-axis in Figure 2i, while the one without an O-vacancy defect is more like a sphere (Figure 2e). The maximum values of bulk modulus of the supercell and supercell with O-vacancy are 53.00 and 67.11 GPa, and the minimum values are 42.25 and 41.02 GPa. The maximum values of the shear modulus of the supercell without and with O-vacancy are 66.11 and 68.10 GPa, and the minimum values are 42.53 and 42.27 GPa. The minimum values of bulk- and shear moduli of α-quartz with and without O-vacancy are similar, while the maximum bulk- and shear moduli of O-vacancy defect α-quartz increased at 21.03 and 2.92% compared without the O-vacancy defect. The O-vacancy defect is more the maximum values of Young's modulus of the supercell and supercell with O-vacancy are 141.81 and 150.82 GPa, and the minimum values are 93.30 and 88.75 GPa. They increased at 5.97 and 4.88%, respectively. This indicated that the O-vacancy defect crystal can increase the compressive strength slightly.

Table 3. Anisotropy Index of the α-Quartz Crystal with and without the O-Vacancy Defect

	A^U	A_B	A_G	A^L
unit cell	0.313	0.214	2.996	0.134
supercell without O-vacancy	0.390	0.330	3.691	0.165
supercell with O-vacancy	0.441	1.106	4.019	0.181

The index of anisotropy calculated by eqs 8 ∼ 10 is shown in Table 3. The calculation of four different anisotropy indexes can show the same tendency that is O-vacancy defect increased the anisotropy of the α-quartz crystal. For A_B, the percentage of the anisotropy index increase about three times, and for A_G, the percentage of the anisotropy index increased by about 8.89%. The effect of the bulk modulus anisotropy index is much more compared to the shear modulus. Whereas, both the A^U and A^L increased by 13.08 and 9.70%.

The bulk-, shear-, and Young's moduli of the low-index cleavage plane are shown in Figure 3. The effect of O-vacancy defects on the bulk modulus of low-index crystalline facets is (010) > (110) > (011) > (111) > (001) > (112) > (100) > (101), which is consistent with the profiles of XRD diffraction peaks of other researches. The effect of O-vacancy defects on the shear modulus of low-index crystalline planes is (011) > (101) > (010) > (110) > (112) > (001) > (100) > (111), which indicates that the exposed surfaces of α-quartz minerals with oxygen defects, under the shear stress, are mainly (011), while the probability existing facets (100) and (111) is a few. The effect of oxygen defects on Young's modulus of low-index crystalline planes is (111) > (010) > (110) > (112) = (100) > (001) > (101), which indicated that the presence of O-vacancy defects has the greatest effect on the compressive strength of (111) facets and (101) facets, which increased the compressive strength of the (111) facet and decreased the compressive strength of the (101) facet.[32] According to the conclusion of this study, the cleavage plane of α-quartz is strongly related to its bulk and shear moduli, and it seems that different force applications (normal, shear stress, and so on) can yield α-

https://doi.org/10.1021/acsomega.3c05173
ACS Omega 2023, 8, 43644−43650

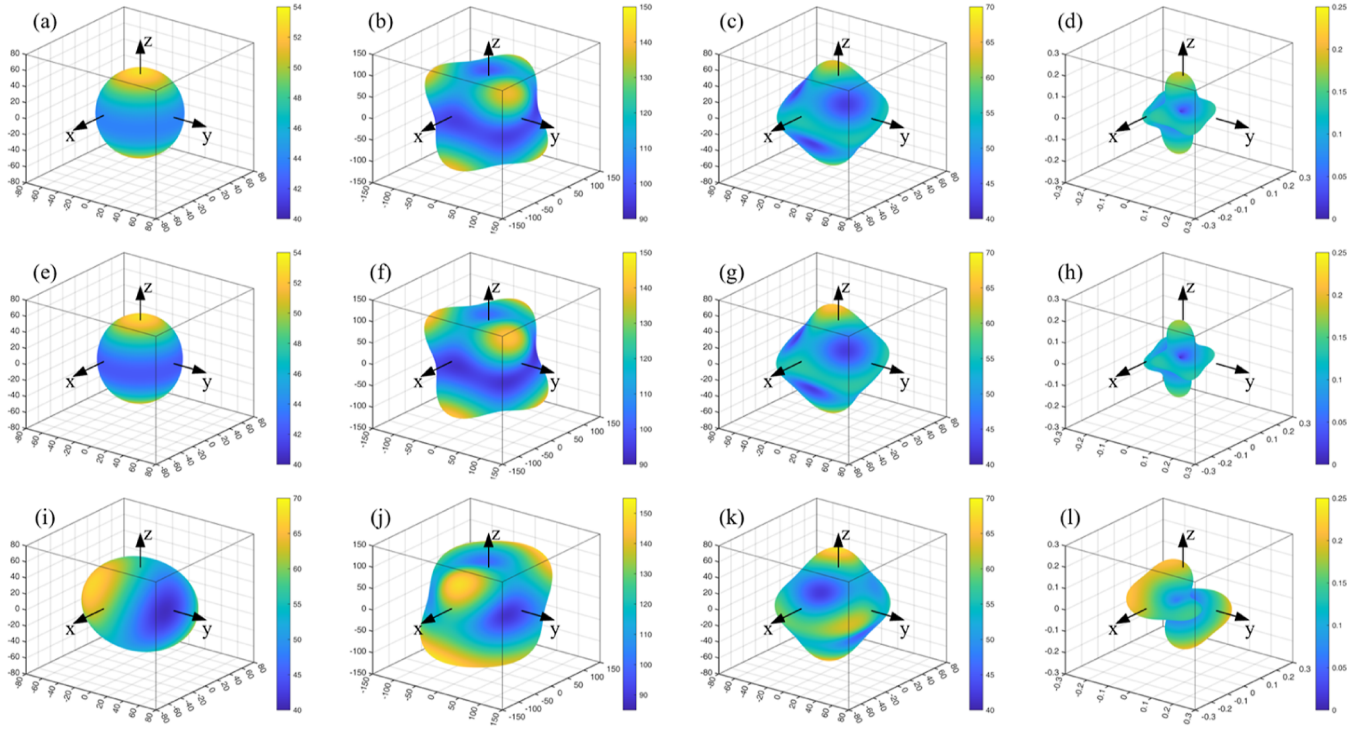

Figure 2. Mechanical properties mapping surfaces of the α-quartz crystal. (The unit of the color bar is GP, except for the Poisson ratio which is dimensionless. The mapping surfaces represent bulk-, Young's-, and shear moduli and Poisson ratio from left to right. (a−d) Unit cell. (e−h) Supercell without an O-vacancy defect. (i−l) Supercell with an O-vacancy defect).

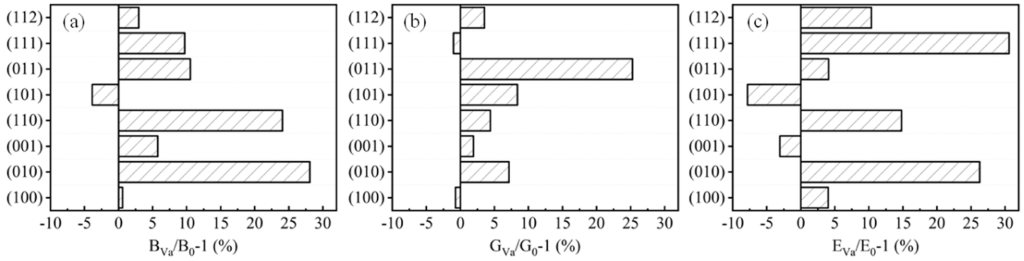

Figure 3. Difference without and with the O-vacancy of bulk modulus (a), (b) shear modulus, and Young's modulus (c). (The subscript Va and 0 represent with O-vacancy and without O-vacancy).

quartz products with different cleavage planes in the grinding process of α-quartz.

2.4. Electron Density Analysis. The features of electron density distributions with and without O-vacancy defects are discussed. For the O-vacancy defect, we calculated the formation of a Si−Si bond, whose length decreased from 3.073 to 2.442 Å (the bond length of silicon bulk is 2.35 Å[33] which is closed); we also find a slight increase of the Si−O bonds adjacent to the vacancy (1.627, 1.637, and 1.630 Å); it is in good agreement with the results of others.[34] This indicates that the defect of the oxygen atom can promote the proximity of adjacent silicon atoms to each other. Figure 4b,d compare cross sections of the valence electron density with- and without O-vacancy defect. The defect of oxygen atoms results in the decrease of electron density in the adjoint region.

In addition, the iso-surfaces of the ELF calculated from the valence electron density are shown in Figure 4a,c. The inner iso-surfaces with isovalue confines two types of domains: one is shared electron domains represented by small, sphere-shared density accumulations between bonded Si and O atoms (shown in white lines), and the other is large cone-shaped and torus-shaped domains near the O atoms, representing electron lone-pair domains. The Mulliken population is shown in Table 4. With the O-vacancy defect, the Mulliken population of forming Si1−Si2 is 0.81. Without O-vacancy defect, the length of Si−Si is 3.07 Å that cannot form a bond,[33] while the bond Si−O is 1.61 Å, and the Mulliken population of Si−O is 0.52.

3. CONCLUSIONS

The relationship between oxygen atom vacancy defects on mechanical properties, the anisotropy of crystal and cleavage planes, and the electron properties, were investigated using the DFT method and supercell approaches.

On the optimized with and without O-vacancy α-quartz crystal, an elastic constant matrix was obtained. The calculated elastic constants show that the O-vacancy defect are mechanically stable while anisotropy is stronger. The elastic properties of the unit cell are similar to the supercell. The with and without O-vacancy defect α-quartz computed bulk moduli were 45.46/52.00 GPa and shear moduli were 52.42/54.74 GPa. Also, Young's moduli were 113.61/121.57 GPa and Poisson ratio were 0.083 and 0.110, respectively.

https://doi.org/10.1021/acsomega.3c05173
ACS Omega 2023, 8, 43644−43650

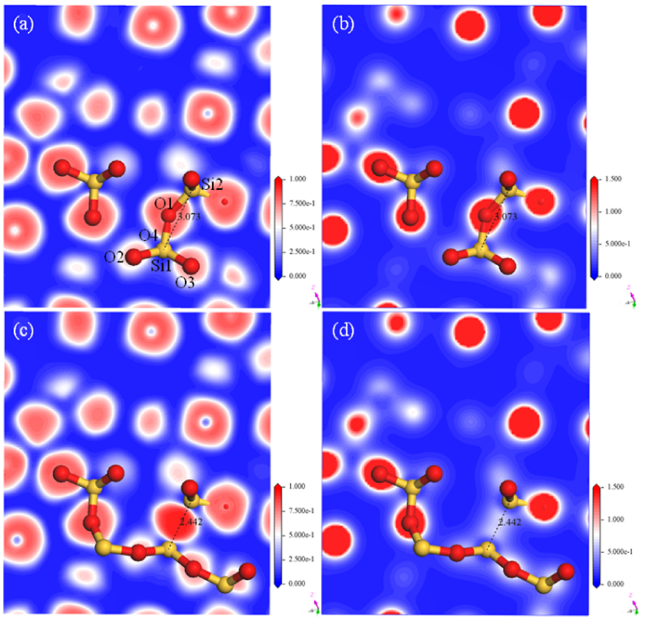

Figure 4. ELF without (a) and with (b) O-vacancy of α-quartz. (The red and yellow spheres represent the oxygen and silicon atoms, respectively).

Table 4. Analysis of the Mulliken Population

	supercell without O-vacancy		supercell with O-vacancy	
	population	length (Å)	population	length (Å)
Si1−O2	0.52	1.61	0.46	1.62
Si1−O3	0.52	1.61	0.44	1.63
Si1−O4	0.52	1.62	0.47	1.63
Si1−O1	0.52	1.61		
Si1−Si2			0.81	2.44

The spatial distributions of bulk, shear, Young's moduli, and Poisson ratio on the crystal surface were revealed by the contours of the computed bulk, shear, Young's moduli, and Poisson ratio. It was suggested that O-vacancy is strongly anisotropic, and the anisotropy index also showed the same tendency, while the A_B, compared with the without O-vacancy defect α-quartz, decreased two times, and the A_G is similar. In the cleavage plane when the applied stress is dominated by normal stress, the order of the effect of O-vacancy defects on the cleavage plane is (010) > (110) > (011) > (111) > (001) > (112) > (100) > (101). When the applied stress is dominated by shear stress, the order of the effect of oxygen defects on the cleavage plane is (011) > (101) > (010) > (110) > (112) > (001) > (100) > (111). The electron density analysis revealed that the O-vacancy defect of α-quartz can decrease the length of Si−Si and also formed the electron trap between the original oxygen atomic site.

4. MATERIALS AND METHODS

4.1. Materials. Pure quartz mineral was obtained from Jiangxi Province, China. The massive pure minerals were hand-selected, crushed, and ground with a clean steel ball mill. Then quartz below 74 μm was obtained by sieving. The X-ray diffraction diagram of quartz is shown in Figure 5, which indicated that the α-quartz had high purity. The lattice parameters obtained by the refinement of XRD data are shown in Table 5.

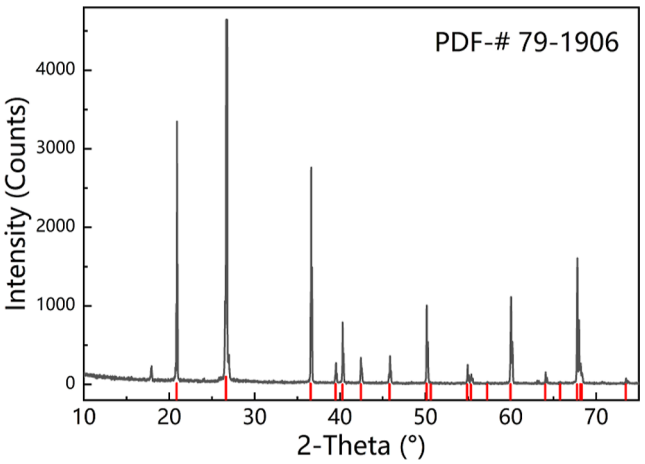

Figure 5. XRD of α-quartz.

4.2. DTF Parameters Setting of Geometry Optimization and Elastic Constants Calculation. The unit cell structure of α-quartz is obtained by Crystallography Open Database (COD)[19] (Figure 1). The chemical formula of the α-quartz unit cell is SiO_2, and its space group is $P3_221$. All calculations in this study were conducted using the CASTEP module. The exchange−correlation convergence tests were performed using mGGA-RSCAN calculations of α-quartz (see Table S1 in the Supporting Information). Due to the subsequent calculation of mechanical properties being sensitive to the calculation parameters, especially the k-point and cutoff energy, more accurate selections of k-point sets and cutoff energies of α-quartz were calculated, and the result was shown in Figure S1 (see Figure S1 in the Supporting Information). After convergence tests, a k-point set of 3 × 3 × 3 and cutoff energy of 570 eV were chosen. The mapping surfaces for bulk-, shear-, Young's moduli, and Poisson ratio were obtained using MATLAB scripts, which were modified by other researchers.[20]

After the validation of crystal parameters in comparison with minerals from pure minerals, the relaxed crystal cell is considered the smallest cell to display the symmetry of the mineral crystal. Then the minimum formation energy of the relaxed cell was calculated and named the final energy hereafter with the unit of eV.

4.3. Calculation of Crystalline Mechanical Properties. The relationship between stress and strain obeys Hooke's law in which the elastic constant can be calculated. The relationship is also expressed with a matrix as follows

$$\begin{bmatrix}\sigma_1\\ \sigma_2\\ \sigma_3\\ \tau_1\\ \tau_2\\ \tau_3\end{bmatrix} = \begin{bmatrix} C_{11} & C_{12} & C_{13} & C_{14} & C_{15} & C_{16}\\ & C_{22} & C_{23} & C_{24} & C_{25} & C_{26}\\ & & C_{33} & C_{34} & C_{35} & C_{36}\\ & & & C_{44} & C_{45} & C_{46}\\ & & & & C_{55} & C_{56}\\ & & & & & C_{66}\end{bmatrix}\begin{bmatrix}\varepsilon_1\\ \varepsilon_2\\ \varepsilon_3\\ \gamma_1\\ \gamma_2\\ \gamma_3\end{bmatrix} \quad (1)$$

where σ, τ, ε, and γ are the normal stress, shear stress, normal strain, and shear strain, respectively. The elastic flexibility matrix was obtained by inverting the elastic stiffness matrix (i.e., $S_{ij} = [C_{ij}]^{-1}$). According to the symmetry of α-quartz, to express the elastic flexibility matrix, there are seven S_{ij} (i.e., S_{11}, S_{12}, S_{13}, S_{14}, S_{33}, S_{44}, and S_{66}).

https://doi.org/10.1021/acsomega.3c05173
ACS Omega 2023, 8, 43644−43650

Table 5. Experiment and Calculated Lattice Parameters of α-Quartz

	α-quartz	$a = b$/(Å)	c/(Å)	volume/(Å^3)
unit cell	experiment	4.90916	5.40216	112.75
	this work	4.93975	5.43625	114.879
	error/%	0.62%	0.63%	1.89%
supercell (2 × 2 × 2)	this work	9.87893	10.8915	920.46
supercell with O-vacancy (2 × 2 × 2)	this work	9.87925	10.8080	907.622

Before calculating bulk-, shear-, Young's moduli, and Poisson's ratios of a lattice, it is important to examine its mechanical stability. For the rhombohedral system, α-quartz, the mechanical stability criteria are as follows[21]

$$C_{11} > |C_{12}|,\ C_{44} > 0,\ C_{13}^2 < \frac{1}{2}C_{33}(C_{11} + C_{12}),\quad C_{14}^2 < \frac{1}{2}C_{44}(C_{11} + C_{12}) \equiv C_{44}C_{66} \tag{2}$$

The Voigt−Reuss−Hill (VRH) moduli based on the VRH approximation depend on the space group of the crystal.[22,23] For the rhombohedral crystal α-quartz, the bulk moduli, B_V and B_R, and shear moduli, G_V and G_R, can be calculated using eqs 3−6, respectively

$$B_V = \frac{(C_{11} + C_{22} + C_{33} + 2C_{12} + 2C_{13} + C_{23})}{9} \tag{3}$$

$$G_V = \frac{(7C_{11} + 5C_{12} + 4C_{13} + 2C_{33} + 12C_{44})}{30} \tag{4}$$

$$B_R = \frac{(C_{11} + C_{12})C_{33} - 2C_{12}^2}{C_{11} + C_{12} + 2C_{33} - 4C_{44}} \tag{5}$$

$$G_R = \frac{5}{2}\frac{[(C_{11} + C_{12})C_{33} - 2C_{12}^2]C_{55}C_{66}}{3B_VC_{55}C_{66} + [(C_{11} + C_{12})C_{33} - 2C_{12}^2]^2(C_{55} + C_{66})} \tag{6}$$

where B_V, B_R, G_V, and G_R are the upper and lower limits of the polycrystalline bulk modulus B and shear modulus G, respectively. The calculated bulk- and shear moduli are the arithmetic average of the two limits. The bulk modulus B and shear modulus G are expressed as follows

$$B = \frac{B_V + B_R}{2},\ G = \frac{G_V + G_R}{2} \tag{7}$$

4.4. Elastic Anisotropy and Hardness. The universal anisotropy index (A^U) proposed by Ranganathan and Ostoja-Starzewski is expressed in eq 8 which is used to describe the anisotropy of the materials.[24] The percentage anisotropy indices of compression and shear (A_B and A_G)[25] are also used to evaluate the elastic anisotropy of a material, and the relationship is expressed as follows

$$A_B = \frac{B_V + B_R}{B_V - B_R} \times 100\%,\ A_G = \frac{G_V - G_R}{G_V + G_R} \times 100\% \tag{8}$$

$$A^U = 5\frac{G_V}{G_B} + \frac{B_V}{B_R} - 6 \tag{9}$$

$$A^L = \sqrt{\left(\ln\left(\frac{B_V}{B_R}\right)\right)^2 + 5\left(\ln\left(\frac{G_V}{G_R}\right)\right)^2} \tag{10}$$

The hardness in terms of the polycrystalline bulk can expressed as follows[26,27]

$$H_V = 0.92k^{1.137}G^{0.708},\ k = \frac{G}{B} \tag{11}$$

$$H_V = 2 \times (G \times k^2)^{0.585} - 3,\ k = \frac{G}{B} \tag{12}$$

■ ASSOCIATED CONTENT

Supporting Information

The Supporting Information is available free of charge at https://pubs.acs.org/doi/10.1021/acsomega.3c05173.

Additional computational details, including convergence tests for cutoff energy and k-points, and determination of the exchange−correlation potentials (PDF)

■ AUTHOR INFORMATION

Corresponding Author

Fen Jiao − *School of Minerals Processing and Bioengineering, Central South University, Changsha 410083, China*; Phone: +86-13549683403; Email: jfen0601@126.com; Fax: +86-0731-88876843

Authors

Lin Zhang − *School of Minerals Processing and Bioengineering, Central South University, Changsha 410083, China*; orcid.org/0000-0002-6183-0476

Wenqing Qin − *School of Minerals Processing and Bioengineering, Central South University, Changsha 410083, China*; orcid.org/0000-0001-5570-9680

Qian Wei − *School of Minerals Processing and Bioengineering, Central South University, Changsha 410083, China*

Complete contact information is available at: https://pubs.acs.org/10.1021/acsomega.3c05173

Notes

The authors declare no competing financial interest.

■ ACKNOWLEDGMENTS

This research was funded by the National Natural Science Foundation of China (grant no. 51974364 and no. 52074355), Key Laboratory of Hunan Province for Clean and Efficient Utilization of Strategic Calcium-containing Mineral Resources (grant no. 2018TP1002), and Co-Innovation Centre for Clean and Efficient Utilization of Strategic Metal Mineral Resources. This work was supported in part by the High Performance Computing Center of Central South University.

https://doi.org/10.1021/acsomega.3c05173
ACS Omega 2023, 8, 43644−43650

REFERENCES

(1) Johnson, S. E.; Song, W. J.; Cook, A. C.; Vel, S. S.; Gerbi, C. C. The Quartz A↔β Phase Transition: Does It Drive Damage and Reaction in Continental Crust? *Earth Planet. Sci. Lett.* **2021**, *553*, 116622.

(2) Massonne, H.-J. A Comparison of the Evolution of Diamondiferous Quartz-Rich Rocks from the Saxonian Erzgebirge and the Kokchetav Massif: Are so-Called Diamondiferous Gneisses Magmatic Rocks? *Earth Planet. Sci. Lett.* **2003**, *216* (3), 347−364.

(3) Bilal, M.; Park, I.; Hornn, V.; Ito, M.; Hassan, F.; Jeon, S.; Hiroyoshi, N. The Challenges and Prospects of Recovering Fine Copper Sulfides from Tailings Using Different Flotation Techniques: A Review. *Minerals* **2022**, *12* (5), 586.

(4) Vieira, A. M.; Peres, A. E. C. The Effect of Amine Type, pH, and Size Range in the Flotation of Quartz. *Miner. Eng.* **2007**, *20* (10), 1008−1013.

(5) Zhou, C.; Liu, L.; Chen, J.; Min, F.; Lu, F. Study on the Influence of Particle Size on the Flotation Separation of Kaolinite and Quartz. *Powder Technol.* **2022**, *408*, 117747.

(6) Feng, Q.; Wen, S.; Zhao, W.; Chen, Y. Effect of Calcium Ions on Adsorption of Sodium Oleate onto Cassiterite and Quartz Surfaces and Implications for Their Flotation Separation. *Sep. Purif. Technol.* **2018**, *200*, 300−306.

(7) Xie, R.; Zhu, Y.; Liu, J.; Li, Y. Effects of Metal Ions on the Flotation Separation of Spodumene from Feldspar and Quartz. *Miner. Eng.* **2021**, *168*, 106931.

(8) Huang, X.; Pang, J.; Zou, J. Study on the Effect of Dry-Wet Cycles on Dynamic Mechanical Properties of Sandstone under Sulfuric Acid Solution. *Rock Mech. Rock Eng.* **2022**, *55* (3), 1253−1269.

(9) Copur, H.; Bilgin, N.; Tuncdemir, H.; Balci, C. A Set of Indices Based on Indentation Tests for Assessment of Rock Cutting Performance and Rock Properties. *J. South Afr. Inst. Min. Metall.* **2003**, *103* (9), 589−599.

(10) Wang, Q.; Li, J.; Yao, G.; Zhu, X.; Hu, S.; Qiu, J.; Chen, P.; Lyu, X. Characterization of the Mechanical Properties and Microcosmic Mechanism of Portland Cement Prepared with Soda Residue. *Constr. Build. Mater.* **2020**, *241*, 117994.

(11) Choyal, V.; Choyal, V. K.; Kundalwal, S. I. Effect of Atom Vacancies on Elastic and Electronic Properties of Transversely Isotropic Boron Nitride Nanotubes: A Comprehensive Computational Study. *Comput. Mater. Sci.* **2019**, *156*, 332−345.

(12) Choyal, V.; Kundalwal, S. I. Effect of Stone-Wales Defects on the Mechanical Behavior of Boron Nitride Nanotubes. *Acta Mech.* **2020**, *231* (10), 4003−4018.

(13) Kothari, R.; Kundalwal, S. I.; Sahu, S. K. Transversely Isotropic Thermal Properties of Carbon Nanotubes Containing Vacancies. *Acta Mech.* **2018**, *229* (7), 2787−2800.

(14) Mo, C.; Zhao, J.; Zhang, D. Real-Time Measurement of Mechanical Behavior of Granite during Heating-Cooling Cycle: A Mineralogical Perspective. *Rock Mech. Rock Eng.* **2022**, *55* (7), 4403−4422.

(15) Sulimov, V. B.; Sushko, P. V.; Edwards, A. H.; Shluger, A. L.; Stoneham, A. M. Asymmetry and long-range character of lattice deformation by neutral oxygen vacancy in α-quartz. *Phys. Rev. B: Condens. Matter Mater. Phys.* **2002**, *66* (2), 024108.

(16) Yuan, Z.; Zhang, C.; Li, L.; Xu, X.; Wang, X. Density Functional Theory Calculation of Fracture Surfaces of Siderite and Hematite. *Powder Technol.* **2020**, *376*, 373−379.

(17) Zhang, C.; Li, L.; Yuan, Z.; Xu, X.; Song, Z.; Zhang, Y. R. Mechanical Properties of Siderite and Hematite from DFT Calculation. *Miner. Eng.* **2020**, *146*, 106107.

(18) Heyliger, P.; Ledbetter, H.; Kim, S. Elastic Constants of Natural Quartz. *J. Acoust. Soc. Am.* **2003**, *114* (2), 644−650.

(19) Gražulis, S.; Daškevič, A.; Merkys, A.; Chateigner, D.; Lutterotti, L.; Quirós, M.; Serebryanaya, N. R.; Moeck, P.; Downs, R. T.; Le Bail, A. Crystallography Open Database (COD): An Open-Access Collection of Crystal Structures and Platform for World-Wide Collaboration. *Nucleic Acids Res.* **2012**, *40* (D1), D420−D427.

(20) Liao, M.; Liu, Y.; Cui, P.; Qu, N.; Zhou, F.; Yang, D.; Han, T.; Lai, Z.; Zhu, J. Modeling of Alloying Effect on Elastic Properties in BCC Nb-Ti-V-Zr Solid Solution: From Unary to Quaternary. *Comput. Mater. Sci.* **2020**, *172*, 109289.

(21) Mouhat, F.; Coudert, F.-X. Necessary and Sufficient Elastic Stability Conditions in Various Crystal Systems. *Phys. Rev. B: Condens. Matter Mater. Phys.* **2014**, *90* (22), 224104.

(22) Nye, J. F.; Nye, J. F. *Physical Properties of Crystals: Their Representation by Tensors and Matrices*; Oxford University Press: Oxford, NY, 1985.

(23) Stefaniuk, D.; Kachanov, M. Voigt-Reuss and Hashin-Shtrikman Bounds Revisited. *Int. J. Eng. Sci.* **2023**, *191*, 103903.

(24) Ranganathan, S. I.; Ostoja-Starzewski, M. Universal Elastic Anisotropy Index. *Phys. Rev. Lett.* **2008**, *101* (5), 055504.

(25) Kube, C. M. Elastic Anisotropy of Crystals. *AIP Adv.* **2016**, *6* (9), 095209.

(26) Tian, Y.; Xu, B.; Zhao, Z. Microscopic Theory of Hardness and Design of Novel Superhard Crystals. *Int. J. Refract. Met. Hard Mater.* **2012**, *33*, 93−106.

(27) Chen, X.-Q.; Niu, H.; Li, D.; Li, Y. Modeling Hardness of Polycrystalline Materials and Bulk Metallic Glasses. *Intermetallics* **2011**, *19* (9), 1275−1281.

(28) Sulimov, V. B.; Pisani, C.; Corà, F.; Sokolov, V. O. Isolated and embedded cluster modelling of the oxygen vacancy in α-quartz. *Solid State Commun.* **1994**, *90* (8), 511−514.

(29) Capron, N.; Carniato, S.; Boureau, G.; Pasturel, A. Study of Oxygen Vacancies in Silica Using Ultra Soft Pseudopotentials. *J. Non-Cryst. Solids* **1999**, *245* (1−3), 146−149.

(30) Song, J.; Corrales, L. R.; Kresse, G.; Jónsson, H. Migration of O vacancies in α-quartz: The effect of excitons and electron holes. *Phys. Rev. B: Condens. Matter Mater. Phys.* **2001**, *64* (13), 134102.

(31) Wu, Z.; Zhao, E.; Xiang, H.; Hao, X.; Liu, X.; Meng, J. Crystal structures and elastic properties of superhard IrN_2 and IrN_3 from first principles. *Phys. Rev. B: Condens. Matter Mater. Phys.* **2007**, *76* (5), 054115.

(32) Bandura, A. V.; Kubicki, J. D.; Sofo, J. O. Periodic Density Functional Theory Study of Water Adsorption on the α-Quartz (101) Surface. *J. Phys. Chem. C* **2011**, *115* (13), 5756−5766.

(33) Wan, W.; Zhang, Q.; Cui, Y.; Wang, E. First Principles Study of Lithium Insertion in Bulk Silicon. *J. Phys.: Condens. Matter* **2010**, *22* (41), 415501.

(34) Roma, G.; Limoge, Y.; Baroni, S. Oxygen Self-Diffusion in α-Quartz. *Phys. Rev. Lett.* **2001**, *86* (20), 4564−4567.

https://doi.org/10.1021/acsomega.3c05173
ACS Omega 2023, 8, 43644−43650